Designing New Small Molecules from Cyclopentadithiophene (CPDT) Derviatives for Highly Efficient Blue Emitters in OLEDs: DFT Computational Modeling

Rania ZAIER[a], Said HAJAJI[a], Masatoshi KOZAKI[b] and Sahbi AYACHI[a]

[a]*Laboratory of Physico-Chemistry of Materials (LR01ES19), Faculty of Sciences of Monastir (FSM), Avenue of the environment 5019 Monastir, University of Monastir, Tunisia.*
[b]*Laboratory of Physical Organic Chemistry, Graduate School of Science, Osaka City University, 3-3-138 Sugimoto, Sumiyoshi-ku, Osaka 558-8585, Japan*

Abstract

Novel blue florescent emitters of two types of linear π-conjugated molecules based on the cyclopentadithiophene (CPDT), having the same backbone but bridging positions with >C=O (**D1**) or >C=C(CN)$_2$ group (**D2**) are designed and theoretically studied. Calculations of the molecular properties of the dimers (**D1** and **D2**) were performed in both ground and excited states using the density functional theory (DFT) and its time-dependent extension (TD-DFT) at B3LYP functional with 6-311g(d,p) basis set in acetonitrile. The optical properties have been computed and data related to their responses are examined and interpreted. The direct comparison between both dimers highlights the effect of carbonyl (>C=O) bridged groups on emission quenching. In addition, intra-molecular charge transfer (ICT) band in the visible region (~672 nm) was detected for **D1**, in contrast to **D2**. The ICT is strongly implicated as the quenching emission caused by the electron-donating (>C=O) group for **D1**. In the three layers based OLED [ITO/NPD/emitting layer (**D1 or D2**)/Alq3/LiF:Al], the electric responses of the devices were evaluated based on the I-V characteristics. Our theoretical results suggest that the CPDT derivatives have interesting optical properties, which are useful for constructing novel light emitting materials for OLEDs.

1. Introduction

Research efforts, over the past several decades, have been devoted to the advancement of organic conjugated systems by an appropriate chemical modification [1-4]. The development of new methodology for the synthesis of short chains, oligomers and polymers gives specifically designed properties for their applications in optoelectronic devices (organic light-emitting diodes (OLEDs) [5-10] and organic solar cells [11-14]). Unfortunately, most OLEDs emitters are still not satisfactory. Therefore, the design and synthesize for new emitting materials with high efficiency have always been one of the biggest challenges in organic electronics [15-18].

Numerous studies have demonstrated that donor-acceptor conjugated systems offer a rational tailoring of the electro-optical properties by the adjustment of the donor (push of electron) and acceptor (pull of electron) units [19-22]. As an effective building block, *4H*-cyclopenta[2,1-*b*:3,4-*b'*]dithiophene (CPDT) has been exploited for constructing the π-conjugated skeleton of organic applications due to its excellent co-planarity and photo-induced electron transfer capability [23, 24].

As a continuation of our previous work [25], we have theoretically studied the CPDT derivatives with two different substituents on the bridging positions to obtain defined and linear π-conjugated systems with small optical band gaps. Connection with electron-donating and accepting groups has been undertaken to control the

fundamental optoelectronic properties of compounds. In other cases, a great deal of attention has therefore been focused on the supramolecular organization in organic conjugated materials by controlling their electronic parameters (optical band gap, energy levels of the highest occupied molecular orbital (HOMO) and the lowest unoccupied molecular orbital (LUMO), effective conjugation length, etc) for desired electronic applications [26].

In order to probe the properties that are difficult to measure and to provide new links necessary for the understanding of the structure-property relationships of materials, the theoretical approach was used as a helpful tool to understand specific phenomena. It also helps scientists make predictions before running the actual experiments. Indeed, theoretical calculations based on the density functional theory (DFT) constitute not only an ideal compromise tool but also an essential analysis method in the same way as other spectroscopic methods of analysis.

Our previous works [25, 27,28] suggested that the DFT/B3LYP method with the 6-311g(d,p) basis set, in solution medium, was reliable for optimization of conjugated systems and its TD-DFT was practical for optical properties simulation.

The current study provides a comparative theoretical analyses related to the optical and electronic properties of organic conjugated homo-dimers containing the *4H*-cyclopenta[2,1-*b*:3,4-*b'*]dithiophen-4-one and the 2-(*4H*-cyclopenta[2,1-*b*:3,4-*b'*]dithiophen-4-ylidene) malononitrile. The dimers under study are, henceforth, referred to as **D1** and **D2**, respectively.
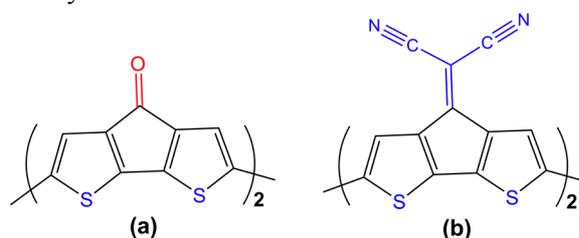
Scheme 1: Molecular structures of **D1** (a) and **D2** (b).

Calculations of molecular properties were performed in both ground and excited states of **D1** and **D2**, in acetonitrile. The vertical excitation energies and oscillator strengths of the first three transitions were computed. In a second step, TD-DFT approach was used to simulate the optical absorption and emission spectra in their respective states. This leads to a consistent and helpful interpretation of the intra-molecular charge transfer (ICT) properties as well as the theoretical design of OLED based **D1** or **D2** as emitting layer. To investigate the charge transport properties, we have calculated the reorganization energies for electron (λ_e) and for hole (λ_h) which are a measure of structural change between ionic and neutral states. We have also calculated the electron density difference (EDD) maps which represent the variation of electron density caused by the charge transfer interactions.

2. Computational details

To perform a theoretical survey on the target OLEDs, some electronic descriptors such as the energy levels of the highest occupied molecular orbital (HOMO), the lowest unoccupied molecular orbital (LUMO), and the energy gap between these molecular orbitals (MOs) have been computed and compared. All the calculations were performed with the Gaussian 09 software [29]. Theoretical calculations for the dimer molecules (**D1** and **D2**) were performed based on the DFT. Internal reorganization energy refers to the energy required for the geometry relaxation when going from the neutral state to a charged molecular state and vice versa [30].

Based on calculations on optimized geometries of the electric neutral, cationic and anionic charged states of the dimer compounds, electronic parameters including the adiabatic ionization potential (IPa), adiabatic electron affinity (EAa) and the reorganization energies were evaluated using the DFT/ B3LYP method with the 6-311g(d,p) basis set, in acetonitrile medium using the conductor-like polarizable continuum model (CPCM). These electronic parameters are an important task to tune the carrier's injection efficiency for OLEDs.

To evaluate the frontier molecular orbitals (FMOs), the ground (S_0) and lowest singlet excited (S_1) states geometries of the compounds are optimized by DFT/B3LYP at 6-311g(d,p) and configuration interaction singles (CIS) methods, respectively. Absorption and emission spectra of both dimers have been calculated at the TD-B3LYP level using the 6-311g(d,p) based on the S_0 and S_1 optimized geometries, respectively.

International Commission on Illumination CIE was used to obtain emission colors coordinates. Finally, the I-V characteristics of OLED devices based dimer (**D1** or **D2**), as emitting layer, have been simulated using SILVACO software [31].

3. Results and discussion

3.1. Geometry changes in excited states

First of all, we can find that both compounds have symmetrical structure and revealed co-planarity between units due to intra-molecular atomic interaction like hydrogen bonds, as depicted S---H (Scheme 2). The highly planar structures due to the presence of intra-molecular non-covalent interactions can apparently increase the rigidity of the molecular backbone [32]. Further, both CPDT structures remain planar in their excited states.
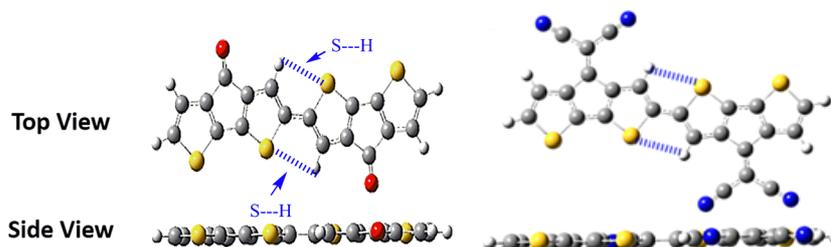
Scheme 2: Optimized geometry of CPDT dimers.

The S-C-C-S dihedrals are obtained to be 179.9° (planar structures) for both **D1** and **D2**. The intra-molecular interactions taking place within the molecular structures generate self-rigidification that improves π-electron delocalization over the conjugated chains. Non-covalent bond lengths of S---H at ground state are found to be 2.91 Å for **D1** and 2.93 Å for **D2** which are rather less than the sum of the van der Waals radii for S (1.80 Å) and H (1.20 Å) at 3.00 Å [33,34]. Moreover, we found that the most sensitive modes to S---H interactions are located approximately at 47 cm^{-1} for **D1** and 34 cm^{-1} for **D2**.

As depicted in Table 1, the dipole moment of both dimers is nearly zero due to the high symmetry of the molecular structures. However, only **D2** exhibits higher dipole moment upon excitation, the value is found at about 4.6 Debye that arise from the efficient bridging group effect. The total energies of **D1** and **D2** at optimized geometries are found to be -2432.96 and -2730.15 Hartree, respectively, indicating that **D2** is more stable regarding the high conjugation of this latter.

Table 1: Calculated total energy and dipole moment at B3LYP/6-311g(d,p) level of dimers at their ground (S_0) and excited (S_1) states

Compounds	Total Energy (Hartree)	Dipole Moment (Debye)
D1	-2432.96 (GS)	0.0009 (GS)
	-2424.98 (ES)	0.0002 (ES)
D2	-2730.15 (GS)	0.0026 (GS)
	-2720.29 (ES)	4.645 (ES)

The different bond lengths of the studied compounds in optimized ground and excited states geometry are illustrated in Fig. 1a (**D1**) and Fig. 1b (**D2**). As it can be seen, there is a slight discrepancy in terms of bond lengths between ground and excited states as a result of modification in electron delocalization within the molecular structures. Particularly, the bond length as numbered 14 (linkage between the two CPDT subunits) is dramatically reduced to form a double bond favoring the ICT between subunits. It is not surprising therefore that upon electronic excitation molecules may adopt equilibrium geometries very different from those in their ground states.
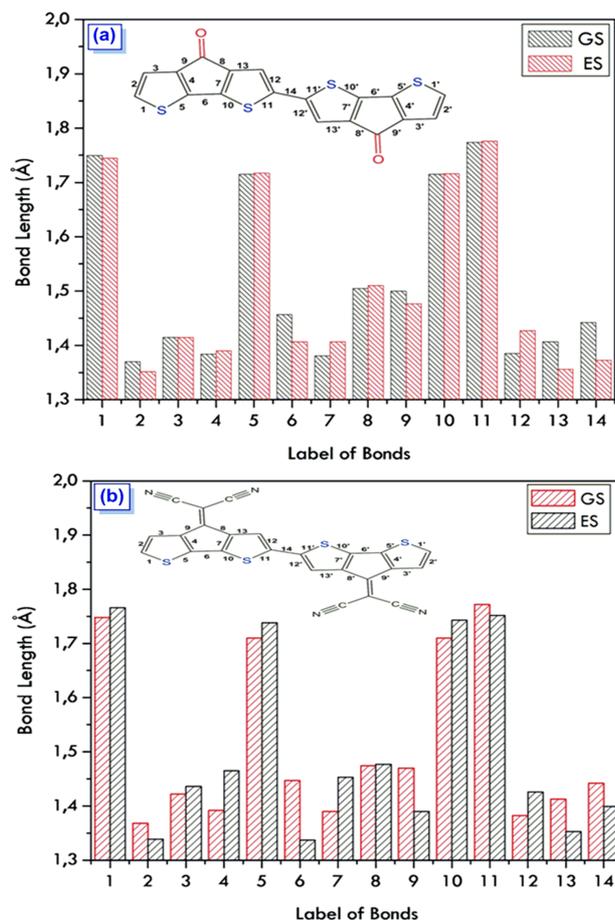
Fig. 1: Bond lengths at optimized ground and excited states of **D1** (1a) and **D2** (1b).

In addition, C=O bond has shortened upon excitation (1.21 Å→1.19 Å) giving an electronic n→π* transition (see after band at 672 nm). From the calculated energies for the excited S_1 states, we can deduce that geometries are slightly decreased in stability regarding their ground S_0 states.

3.2. The Frontier Molecular Orbital (FMO) energy levels and band gaps

To further determine the energy levels of frontier orbitals, Fig. 2 illustrates the electronic energy level diagrams of the studied dimers as well as their FMOs in the ground states. We conclude that the HOMO electrons in both dimers are predominantly distributed on the entire framework of the CPDT, expect contributions from the bridging groups. This result implies that such systems can be considered as highly conjugated configurations. On the other hand, the LUMO electrons are delocalized over whole dimer molecules and the good overlap between subunits can facilitate the electron migration.
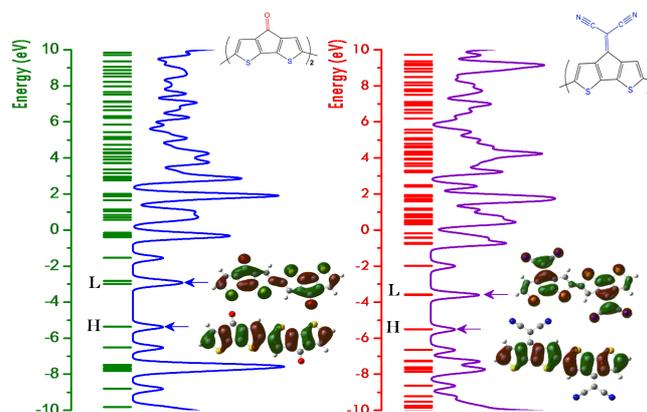
Fig. 2: Frontier molecular orbitals (FMOs) and energy levels at ground state using DFT/B3LYP/6-311g(d,p) method.

In excited states of dimers, we find that no appreciable changes of FMOs were detected for **D1**. Unfortunately, in the case of dimer **D2**, exclusively one of CPDT moiety contributes to the LUMO orbital (see Fig. 3), thanks to electron acceptor character of $>C=C(CN)_2$ group.
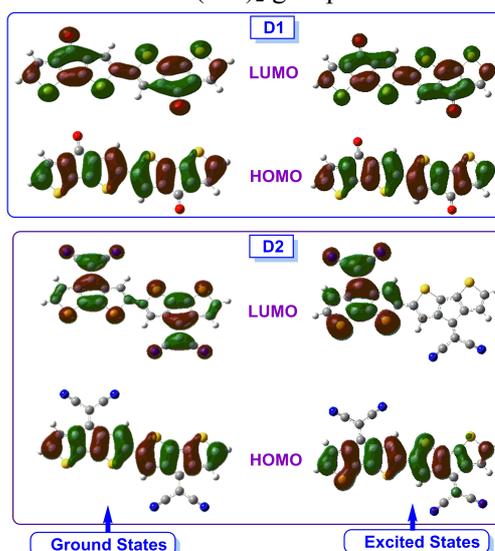
Fig. 3: Frontier orbitals illustrated at the optimized ground (S_0) and excited (S_1) state geometries of the dimers molecules obtained DFT// and TD-DFT//B3LYP/6-31g(d,p) levels of theory, respectively.

The optical energy gap separating the HOMO/LUMO energy levels of **D1** and **D2** are calculated and illustrated in Table 2. We deduce that relatively small optical gap was obtained in the case of **D2** (1.91 eV) compared to **D1** (2.38 eV). Since the HOMOs have a nodal plane at the bridging carbon atom in the CPDT, electron withdrawing groups at the bridging carbon selectively stabilize the LUMOs. This is a reason for the narrow band gaps of these compounds.

Table 2: Calculated energetic parameters at DFT//B3LYP/6-311g (d,p) level.

Compunds	ε_{HOMO} (eV)	ε_{LUMO} (eV)	ΔE_{gap} (eV)	ε_{HOMO-1} (eV)	ε_{HOMO+1} (eV)
D1	-5.36	-2.98	2.38	-6.51	-2.82
D2	-5.51	-3.60	1.91	-6.65	-3.58

The FMOs analysis has turned out that the vertical electronic transitions of absorption and emission of both dimers are characterized as ICT [35, 36]. This latter arising from the electron transition from the HOMO to the LUMO indicates the formation of charge density difference between ground (S_0) and excited (S_1) states that can be visualized through the electronic density difference (EDD) plots. The major changes in EDD, which are reflected in atomic charges, should be apparent in the molecular electrostatic potential (MEP) that derived an analysis of electron density. Here, the EDD plots of the studied compounds have been illustrated in Fig. 4. As displayed in the figure, the regions of the electron density depletion presented in blue color are mostly localized at the donor parts, while the regions of the electron density increment presented in purple color are largely aligned with the acceptor parts [37,38].
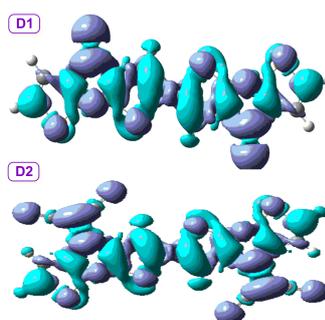
Fig. 4: Electron density difference (EDD) isosurface maps between ground (S0) and excited (S1) states of **D1** and **D2**.

3.3. Molecular Electrostatic Potential (M.E.P) Maps and Mulliken population analysis

The Mulliken charges and surface electrostatic potentials usually shed light on the electron distribution and electrostatic interaction within molecules. Therefore, molecular electrostatic potential (M.E.P) is a useful descriptor for understanding the reactive sites of electrophilic and nucleophilic attacks of the studied molecules as long as it is directly related to the electron density [39]. To predict the different reactive sites of **D1** and **D2**, the M.E.P calculated at B3LYP/6-311g(d,p) at optimized geometries have been simulated and depicted in Fig. 5. The negative regions of M.E.P, represented in red color, are referring to electrophilic reactivity and the positive regions that are produced in white color are related to nucleophilic attack. In ground states of dimers, the symmetric charge distribution gives a partially positively charge CPDT and a negatively charged bridging groups (in periphery).
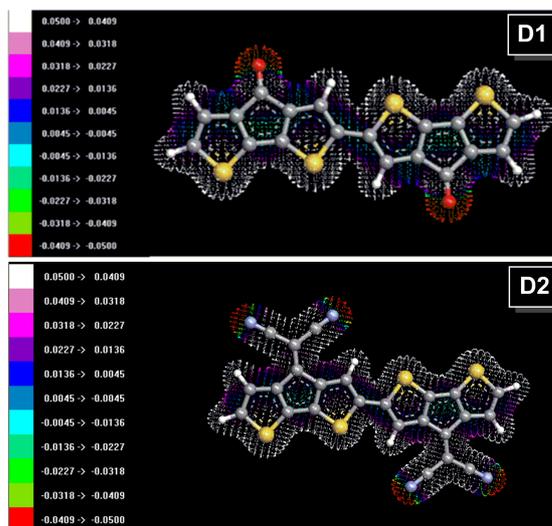
Fig. 5: Molecular electrostatic potential surface (MEP) of **D1** and **D2**.

To make easy the interpretation of the charge distribution, we have calculated the Mulliken atomic charges over the different molecular domains for the two CPDT molecules (Fig. 6). It is worth remembering that the two CPDT structures with symmetric geometries are planar. Here, the net charges over the CPDT moiety and bridging groups are also identical in their ground states, but affected upon excitation.

As shown, in their ground states, the partial negative charges are on the $>C=C(CN)_2$ bridging groups. In turn, the partial positive charges are spread on the CPDT backbone, for both dimer molecules. When regarding excited states of molecules, a redistribution of electronic charges was detected. The arrangements can potentially result in a strong π-π interaction within the CPDT fragments. These results show qualitative agreement with the results based on the FMOs analysis.
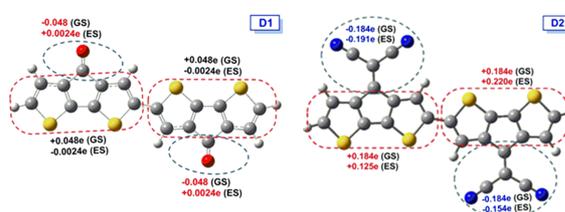
Fig. 6: Mulliken atomic charges distribution at ground (S_0) and excited (S_1) states of **D1** and **D2**.

3.4. Optical responses (UV-Vis-NIR optical absorption and emission)

The absorption properties of the titled compounds based on UV-Vis-NIR spectra are displayed in Fig. 7. The data related with their behaviors are listed in Table 3. First of all, the UV-vis-NIR spectra have three distinct absorptions peaks appeared at 312, 372 and 672 nm for **D1**. However, the detected peaks are red-shifted and appeared at 359, 394 and 946 nm for the **D2**.
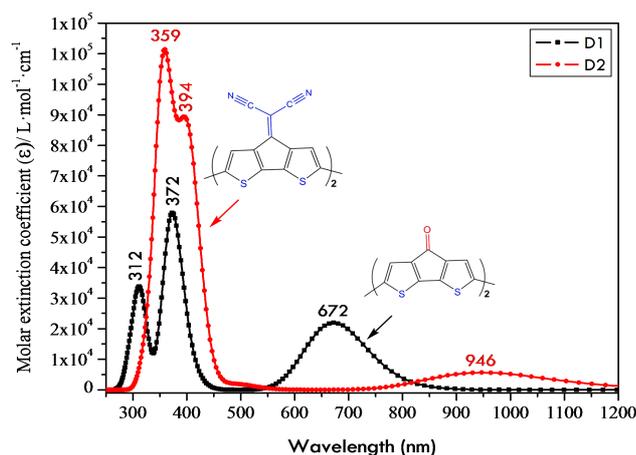
Fig. 7: Simulated optical absorption spectra of dimer molecules at TD-DFT//B3LYP/6-311g(d,p) level of theory.

Table 3: The vertical excited energies (nm) and their oscillator strengths for the ground ($S_0 \rightarrow S_1$) states of dimers by TD//B3LYP/6-311g(d,p) level of theory.

Compounds	λ_{max}^{Abs}(nm)	E(eV)	f (a.u)	Main Transition
D1	312	3.97	0.4099	H-4→L (55%)
	394	3.33	0.7592	H→L+2 (93%)
	672	1.84	0.3026	H→L (96%)
D2	359	3.47	0.7434	H-2→L+1 (28%)
	394	3.08	1.0941	H→L+2 (93%)
	946	1.31	0.0780	H→L (96%)

Additionally, compared to **D2**, a dramatic hypo-chromic effect was observed in UV-vis-NIR spectrum of **D1**. Logically speaking, the changes are closely related to their molecular properties arising from electron withdrawing and donating group's effect. We will return later to this point. For **D2**, the selective stabilization of the LUMO by the bridging groups is important. Then, the stronger electron withdrawing group gives stronger stabilization effect. The simulation of resolved emission spectra is illustrated in Fig. 8. The corresponding emission properties are summarized in Table 4.
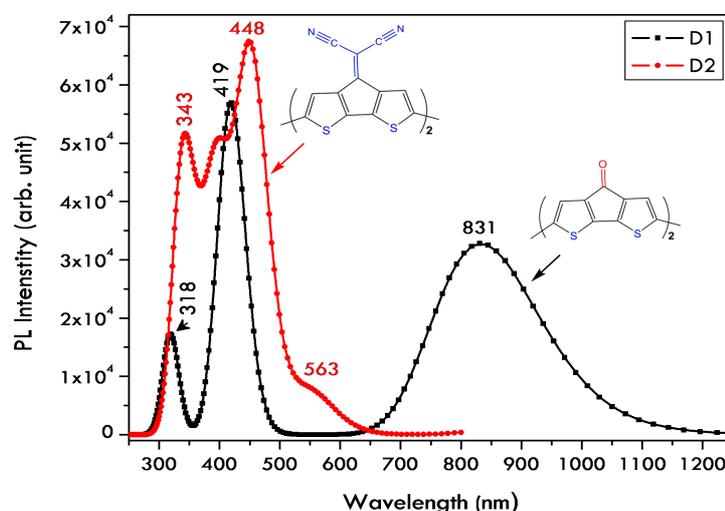
Fig. 8: Simulated emission spectra of dimer molecules at TD-DFT//B3LYP/6-311g(d,p) level of theory.

Table 4: The vertical emission energies (nm) and their oscillator strengths for the first excited ($S_1 \rightarrow S_0$) states of dimers by TD//B3LYP/6-311g(d,p) level of theory.

Compounds	λ_{max}^{Em}(nm)	E_{flu} (eV)	f (a.u)	Main Transition	τ (ns)
D1	319	3.88	0.2147	L→H-5 (81%)	
	419	2.96	0.7543	L+2→H (95%)	3.49
	831	1.50	0.4528	L→H (97%)	
D2	334	3.5987	0.2351	L+1 → H-3 (51%)	
	389	3.1061	0.4341	L → H-2 (42%)	
	448	2.7426	0.8754	L+2 → H (79%)	3.51
	563	2.2583	0.1009	L→ H-1 (92%)	

From the obtained results, it is worth noting that **D1**-spectrum is strongly influenced by electron transfer processes. For comparison's sake to **D1**, **D2** shows a hyper- and bathochromic effect for wavelengths less than 500 nm. The observed bands for **D1** (318 and 419 nm) are shifted by + 25 nm for **D2**. Besides, a lowest intensity band has been detected at about 563 nm for **D2**. From optical responses, certainly, the carbonyl (C=O) with donating group is responsible for the efficient quenching of emission. ICT caused by strongly electron donating/accepting character interacting substituent is important in governing the optical responses [40-42].

To make easy the interpretation of the optical responses of the dimer compounds under study, the emission spectra have been fitted by mean of Gaussian peaks for both **D1** and **D2**. As illustrated in Fig. 9, the PL spectrum of **D1** displays two distinct bands noted (1) and (2) for wavelength above 500 nm. However, for the **D2**, the emission spectrum shows three optical bands in the same region.
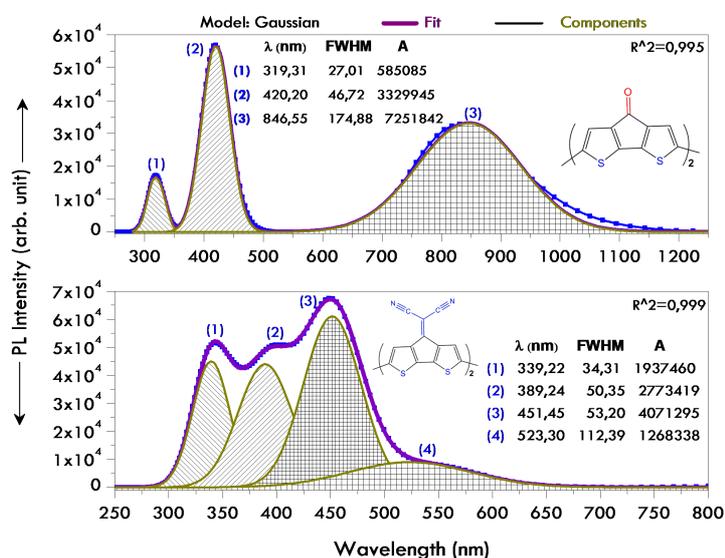
Fig. 9: Fitting Gaussian peaks of emission spectra. The FWHM and A are the full width at half maximum and analytical integration, respectively.

In addition, a significant emission band in the near infrared domain has detected for **D1** (band (3)). In contrast, relatively lower band was observed at 523 nm (band (4)) for the **D2**. This letter result can be attributed to excited state ICT. Their corresponding rate of analytic integration is $\frac{A_{(4)}(D2)}{A_3(D1)} \approx 17.5\%$. Accordingly, the carbonyl bridging strongly affect the emission response leading to a quenching effect.

The optical properties of the compounds based on UV-Vis-NIR and PL spectra together with the high oscillator strengths are depicted in Fig. 10 for further understanding the optical properties of the dimer molecules.
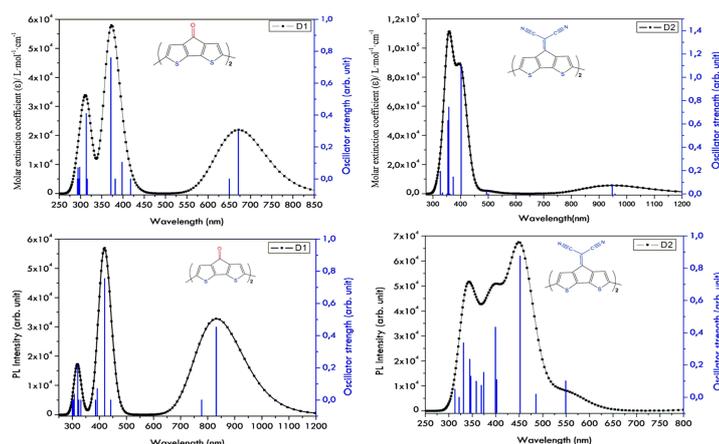
Fig. 10: Absorption and emission spectra with oscillator strength (vertical lines) of the investigated compounds.

In order to understand the role played by the carbonyl group as push of electron, we have calculated the radiative lifetime for both dimers for the sake of comparison. Radiative lifetime (τ) define the average time of the molecule stay at the excited state before emission a photon, which means that lower is the value of τ the more efficient is the emission of the compound. The radiative lifetime can be calculated using the following expression [43]:

$$\tau = \frac{C^3}{2(E_{flu})^2 f}$$

Where C is the velocity of light, E_{flu} is the fluorescent energy and f is the oscillator strength.

The radiative lifetime values are calculated to be 3.49 ns and 3.51 ns for **D1** and **D2**, respectively. Surprisingly, the obtained results reveal that compound **D1** exhibits a radiative life time relatively lower than **D2**, which indicates that **D1** has more efficiency in the emission of photons. From energy level diagrams, the LUMO was evaluated about -2.98 eV and -3.60 eV, for **D1** and **D2**, respectively. The oscillator strength of the HOMO→LUMO transition is important factor for the efficient ICT, upon photo excitation. In turn, the lower radiative lifetime is strictly related to this process. A considerable increase in the excited state dipole moment compared to ground state dipole moment is certainly related substantial redistribution of π-electron densities in a more polar excited state for the **D2** dimer.

3.5. Charge transport and related properties

Designing an efficient multilayer structure requires knowing the precise energy of the hole and electron transport levels of constituent materials. As mentioned in the introduction part, the reorganization energy could be an important factor that governs the mobility of charge carriers. Then, as referred to [44], the reorganization energies for electron (λ_e) and for hole (λ_h) transfer can be defined as:

$$\lambda_e = (E_0^- - E_-^-) + (E_-^0 - E_0^0) \qquad (1)$$
$$(\lambda_h = (E_0^+ - E_+^+) + (E_+^0 - E_0^0) \qquad (2)$$

Where $E_0^+ (E_0^-)$ is the energy of the cation (anion), calculated with the optimized structure of the neutral molecule and $E_+^+ (E_-^-)$ is the energy of the cation (anion), calculated with the optimized cation (anion) structure. The $E_+^0 (E_-^0)$ is the energy of the neutral molecule calculated at the cationic (anionic) state. Whereas, E_0^0 represent the energy of the neutral molecule at the ground state.

The calculated mobility of charge carriers (λ_e and (λ_h) are reported in Table 5. From the obtained results, we conclude that **D2** possesses a high charge transfer ability regarding the large balance of reorganization energy for hole ((λ_h = 0.309) and electron (λ_e = 0.305), unlike **D1**, where we find that the reorganization energies values are of 0.311 for hole and 0.503 for electron.

Table 5: Reorganization energies λ (eV) for hole (λ_h) and electron (λ_e) transport and other electronic parameters expressed in eV calculated at B3LYP/6-311g(d,p) level of theory.

Compounds	$(E_0^+ - E_+^+)$	$(E_+^0 - E_0^0)$	$(E_0^- - E_-^-)$	$(E_-^0 - E_0^0)$	λ_h	λ_e	IPa	EAa	η
D1	0.155	0.155	0.182	0.321	0.311	0.503	5.09	3.24	0.925
D2	0.154	0.156	0.156	0.149	0.309	0.305	5.21	3.87	0.670

It is well know that electronic parameters including the adiabatic ionization potential (IPa) and adiabatic electron affinity (EAa) determination are important task to tune the carriers injection efficiency for OLEDs [45]. The values of IPa and EAa were calculated as described in equations below:

$$IPa = E(M^+) - E(M^0) \qquad (3)$$

$$EAa = E(M^0) - E(M^-) \qquad (4)$$

Where $E(M^0)$, $E(M^+)$ and $E(M^-)$ are the total energies of the neutral, cationic (RC) and anionic forms of the molecules, respectively. μνλθσδφγηη

Using the above mentioned parameters, we could predict the stability of the compounds through the calculation of their absolute hardness as denoted η and given by: $\eta = \frac{IPa - EAa}{2}$ (5).

The determined energy parameters represent the energy levels relevant to the OLED performance. From Table 5; we note that both dimer molecules exhibit almost the same values of IPa but distinct values of EAa.

As known, the global hardness η measures the stability of a system in terms of resistance to electron transfer [46]. In our case, the obtained values are 0.925 eV for **D1** and 0.670 eV for **D2**. This clearly reveals that the **D2** dimer exhibits relatively high stability, implying that the bridging groups has significantly affect the stability of the CPDT derivatives.

3.6. Organic Light Emitting Diodes (OLEDs) modulation

The analysis of IPa, EAa and reorganization energy shows the high performance of hole and electron mobility that leads to a high color quality and efficient electroluminescent devices. As illustrated in Fig. 11, the simulated CIE coordinates were found to be (0.16, 0.04) for **D1** and (0.16, 0.09) for **D2**, corresponding to blue emission [47]. It resulted in the enhancement of luminescent efficiency.
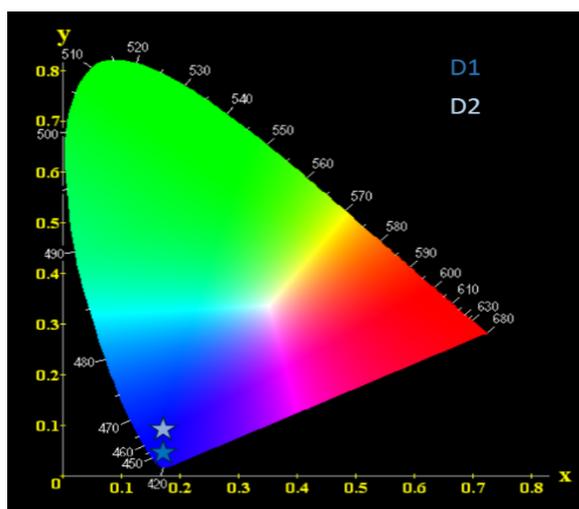
Fig. 11: The representative CIE color coordinates of **D1** and **D2**.

Multilayer OLEDs can be viewed as two or more layers in order to improve device efficiency. As well as conductive properties, different materials may be chosen to aid charge injection at electrodes. However, a common way to balance charge is optimizing the thickness of the charge transporting layers which is hard to control.

As already proposed for the appropriate layers (HIL and EIL with optimal values of the thickness) to improve the efficiency of carriers injection [25] based on their energy levels diagram (HOMO and LUMO) [48-50], typical OLED device architecture is depicted in Fig. 12.
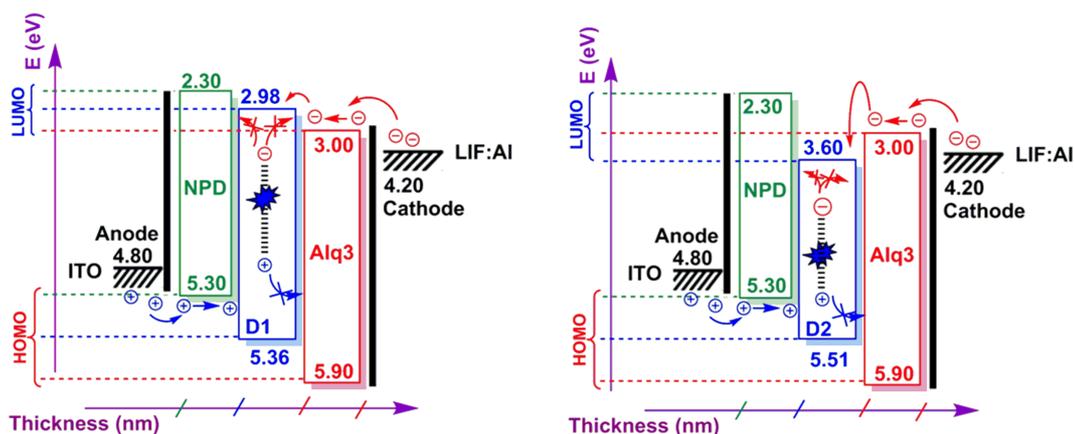
Fig. 12: Typical OLEDs architecture including **D1** and **D2** as emitting layers.

In the three layers based OLED, the insertion of HIL and EIl layers of charge transport materials in addition to the emitter layer (CPDT derivatives) provides a powerful means to control charge injection, transport and recombination in OLEDs. It is worth remembering that a large barrier for charge injection results in high driving voltage, and unipolar charge-transport capability leads to unbalanced charge transport and consequently low recombination efficiency. In our case, the ultrahigh electron mobility of Alq3 favorites the electron transport and the deep HOMO level (ε_{HOMO} = 5.9 eV) prevents efficiently the hole leakage from the emitting layer. Further, the small HOMO barrier of NPD (ε_{HOMO} = 5.3 eV) allows hole injection to efficiently reach the emitting layer.

For practical application, we believe that CPDT derivatives with highly planar structures that possess designed supra-molecular interactions, such as $\pi \rightarrow \pi$ stacking, can greatly enhance the efficiency and stability of electroluminescence (EL).

3.7. Characteristics current-voltage (I-V)

The electrical responses of the two kinds of devices, simulated using SILVACO software package, were evaluated based on the current-voltage (I-V) characteristics and results were plotted in Fig. 13. Typical voltages required to turn OLED devices were closed to 4.6 V for **D1** and 7.6 V for **D2**. It is obviously that the relatively lower operating voltage was related to the efficient electron injection within device based **D1** emitting layer.
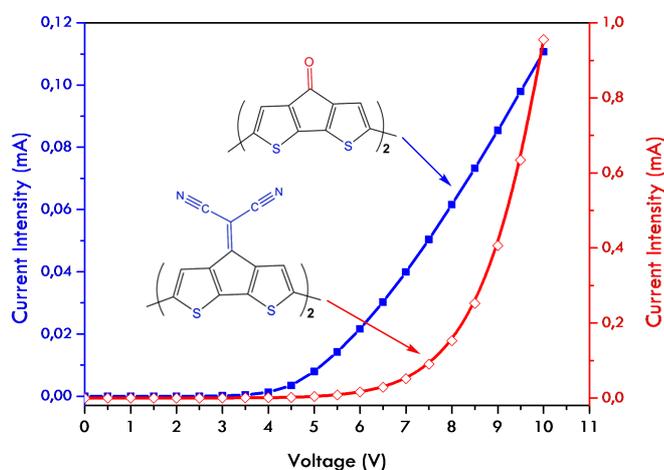
Fig. 13: Current-voltage characteristics of devices.

Conclusion

Two types of π-conjugated CPDT derivatives with small band gaps, were deeply investigated through theoretical calculations based on the Density Functional Theory (DFT) and its Time-Dependent extension (TD-DFT) at B3LYP functional with 6-311g(d,p) basis set in acetonitrile. We have demonstrated that a push-pull effect is certainly expected in these molecules. Especially, the direct comparison between both dimers highlights the effect of carbonyl (>C=O) bridged groups on emission quenching effect and blue-shifted of the optical responses due to the photo-induced electron transfer. From optical absorption responses, both dimers exhibit a relatively narrow band gap (2.38 eV for **D1** and 1.91 eV for **D2**) and low lying energy levels with the HOMO of -5.36 and -5.51 eV, respectively.

From PL spectra analysis, the studied compounds exhibit an emission in the blue region (419 nm (**D1**) and 451 nm (**D2**). The results are supported by CIE coordinates, in which values are determined to be (0.16, 0.04) for **D1** and (0.16, 0.09) for **D2** that are strongly located in the blue region.

From the calculated results of reorganization energies, we have demonstrated that compounds exhibit high performance for charge mobility. Further, current-voltage characteristic has been also simulated. The threshold voltages are found to be 4.6 V for **D1** and 7.6 V for **D2**. Accordingly, both dimers of molecule have excellent optical properties and electrical characteristics that make them attractive candidates for designing functional materials to be used as active layer in OLED devices. Therefore, continuous efforts have been devoted to design and synthesize high performance deep-blue emitters.

References

1. X. Guo, M. Baumgarten, K. Müllen, *Progress in Polymer Science* 38 (2013) 1832.
2. S.C. Rasmussen, S.J. Evenson, C.B. McCausland, *Chem. Commun.* 51 (2015) 4528.
3. L. Liu, G. Yang, X. Tang, Y. Geng, Y. Wu, Z. Su, *J. Mol. Graph. Model.* 51 (2014) 79.
4. M.E. Cinar, T. Ozturk, *Chem. Rev.* 115 (2015) 3036.
5. M. Jung, J. Lee, H. Jung, S. Kang, A. Wakamiya, J. Park, *Dyes Pigments* 158 (2018) 42.
6. S.F. Varol, S. Sayin, S. Eymur, Z. Merdan, D. Ünal, *Org. Electron.* 31 (2016) 25.
7. G. Krucaite, U. Baranauskyte, D. Tavgeniene, V. Andruleviciute, S. Sutkuviene, B. Yao, Z. Xie, B. Zhang, S. Grigalevicius, *Opt. Mater.* 72 (2017) 583.
8. A. Irfan, F. Ijaz, A. G. Al-Sehemi, A. M. Asiri, *J. Comp. Elec.* 11 (4) (2012) 374.
9. K. Nimith, M. Satyanarayan, G. Umesh, *Opt. Mater.* 80 (2018) 143.
10. X. Li, H.-J. Chi, G.-H. Lu, G.-Y. Xiao, Y. Dong, D.-Y. Zhang, Z.-Q. Zhang, Z.-Z. Hu, *Org. Electron.* 13 (2012) 3138.
11. J. Sun, S. Venkatesan, A. Dubey, Q. Qiao, C. Zhang, *Journal of Polymer Science Part A: Polymer Chemistry* 55 (2017) 1077.
12. L. Zhang, W. Shen, R. He, X. Liu, X. Tang, Y. Yang, M. Li, *Org. Electron.* 32 (2016) 134.
13. J. Sun, X. Ma, Z. Zhang, J. Yu, J. Zhou, X. Yin, L. Yang, R. Geng, R. Zhu, F. Zhang, *Adv. Mater.* 30 (2018) 1707150.
14. M. Ans, J. Iqbal, B. Eliasson, K. Ayub, *Comput. Mater. Sci.* 159 (2019) 150.
15. M. Zhu, C. Yang, *Chem. Sci. Rev.* 42 (2013) 4963.
16. S.S. Reddy, V.G. Sree, H.-Y. Park, A. Maheshwaran, M. Song, S.-H. Jin, *Dyes Pigments* 145 (2017) 63.
17. S. Ayachi, A. Mabrouk, M. Bouachrine and K. Alimi (November 14th 2012). Photophysical Properties of Two New Donor-Acceptor Conjugated Copolymers and Their Model Compounds: Applications in Polymer Light Emitting Diodes (PLEDs) and Polymer Photovoltaic Cells (PPCs), *Organic Light Emitting Devices*, Jai Singh, IntechOpen, DOI: 10.5772/54254. Available from: https://www.intechopen.com/books/organic-light-emitting-devices.
18. G. Turkoglu, M. Cinar, A. Buyruk, E. Tekin, S. Mucur, K. Kaya, T. Ozturk, J. Mater. Chem. C. 4 (2016) 6045.
19. J.D. Azoulay, Z.A. Koretz, B.M. Wong, G.C. Bazan, *Macromolecules* 46 (2013) 1337.
20. Y. Zhang, L. Zhang, R. Wang, X. Pan, *J. Mol. Graph. Model.* 34 (2012) 46.
21. P. Ledwon, P. Zassowski, T. Jarosz, M. Lapkowski, P. Wagner, V. Cherpak, P. Stakhira, *J. Mater. Chem. C.* 4 (2016) 2219.
22. B. Grimm, C. Risko, J.D. Azoulay, J.-L. Brédas, G.C. Bazan, *Chem. Sci.* 4 (2013) 1807.
23. P. Coppo, M.L. Turner, *J. Mater. Chem.* 15 (2005) 1123.

24. H. Hanamura, N. Nemoto, *Polymer* 52 (2011) 5282.
25. R. Zaier, S. Hajaji, M. Kozaki and S. Ayachi, Opt. Mat. 91 (2019) 108.
26. C. Zhang, J. Sun, Q. Qiao, J. Li, Polymer 55 (2014) 4677.
27. F. Mahdhaoui, R. Zaier, N. Dhahri, S. Ayachi, T. Boubaker, *Int J Chem Kinet.* 2019;1–9 (https://doi.org/10.1002/kin.21247).
28. R. Zaier, F. Mahdhaoui, S. Ayachi, T. Boubaker, *J. Mol. Struct.* 1182 (2019) 131.
29. Gaussian 09, Revision A.1, M. J. Frisch, G. W. Trucks, H. B. Schlegel, G. E. Scuseria, M. A. Robb, J. R. Cheeseman, G. Scalmani, V. Barone, B. Mennucci, G. A. Petersson, H. Nakatsuji, M. Caricato, X. Li, H. P. Hratchian, A. F. Izmaylov, J. Bloino, G. Zheng, J. L. Sonnenberg, M. Hada, M. Ehara, K. Toyota, R. Fukuda, J. Hasegawa, M. Ishida, T. Nakajima, Y. Honda, O. Kitao, H. Nakai, T. Vreven, J. A. Montgomery, Jr., J. E. Peralta, F. Ogliaro, M. Bearpark, J. J. Heyd, E. Brothers, K. N. Kudin, V. N. Staroverov, R. Kobayashi, J. Normand, K. Raghavachari, A. Rendell, J. C. Burant, S. S. Iyengar, J. Tomasi, M. Cossi, N. Rega, J. M. Millam, M. Klene, J. E. Knox, J. B. Cross, V. Bakken, C. Adamo, J. Jaramillo, R. Gomperts, R. E. Stratmann, O. Yazyev, A. J. Austin, R. Cammi, C. Pomelli, J. W. Ochterski, R. L. Martin, K. Morokuma, V. G. Zakrzewski, G. A. Voth, P. Salvador, J. J. Dannenberg, S. Dapprich, A. D. Daniels, O. Farkas, J. B. Foresman, J. V. Ortiz, J. Cioslowski, and D. J. Fox, Gaussian, Inc., Wallingford CT, 2009.
30. T. Matsushima, C. Adachi, Chem. Mater. 20 (2008) 2881.
31. Silvaco Int., Atlas User's Manual [online], Available at www.silvaco.com.
32. M.H. Hoang, D.N. Nguyen, T.T. Ngo, H.A. Um, M.J. Cho, D.H. Choi, Polymer 83 (2016) 77.
33. G.P. Schiemenz, *Zeitschrift für Naturforschung B*. 62 (2007) 235.
34. N.E. Jackson, B.M. Savoie, K.L. Kohlstedt, M. Olvera de la Cruz, G.C. Schatz, L.X. Chen, M.A. Ratner, *J. Am. Chem. Soc.* 135 (2013) 10475.
35. X. Wang, A. Tang, F. Chen, E. Zhou, *Polymer* 167 (2019) 31-39.
36. Y. Zhou, M. Zhang, J. Ye, H. Liu, K. Wang, Y. Yuan, Y.-Q. Du, C. Zhang, C.-J. Zheng, X.-H. Zhang, *Org. Electron.* 65 (2019) 110.
37. Z. Xu, Y. Li, W. Zhang, S. Yuan, L. Hao, T. Xu, X. Lu, *Spectrochim. Acta A*. 212 (2019) 272.
38. A. Ostovan, Z. Mahdavifar, M. Bamdad, *Polymer* 126 (2017) 162.
39. X. Wen, Y. Yin, Y. Li, S. Liu, L. Zhang, N. Ma, G. Shan, W. Xie, *Org. Electron.* 15 (2014) 675.
40. V. Ramkumar, P. Kannan, *Opt. Mat.* 46 (2015) 314.
41. C.-Y. Tseng, F. Taufany, S. Nachimuthu, J.-C. Jiang, D.-J. Liaw, *Org. Electron.* 15 (2014) 1205.
42. P. Willot, L. De Cremer, G. Koeckelberghs, Macromol. *Chem. Phys.* 213 (2012) 1216.
43. S. Jungsuttiwong, R. Tarsang, Y. Surakhot, J. Khunchalee, T. Sudyoadsuk, V. Promarak, S. Namuangruk, *Org. Electron.* 13 (2012) 1836.
44. M.S. Stark, *J. Phys. Chem. A*. 101 (1997) 8296.
45. L.Y. Zou, A.M. Ren, J.K. Feng, X.Q. Ran, Y.L. Liu, C.C. Sun, Int. *J. Quantum Chem*. 109 (2009) 1419.
46. R. Vivas-Reyes, F. Núñez-Zarur, E. Martı, *Org. Electron.* 9 (2008) 625.
47. Z. Li, G. Gan, Z. Ling, K. Guo, C. Si, X. Lv, H. Wang, B. Wei, Y. Hao, *Org. Electron.* 66 (2019) 24.

(2019) ; http://www.jmaterenvironsci.com